Anomalous reflection beam steering based on high-bit coding metasurfaces

FENG LIN[1], WENKANG HUANG[1], XUEJUN HE[1], CHENXIA LI[2,*]
[1]*Zhejiang Institute of Economics & Trade, Hangzhou 310018, China*
[2]*Institute of Optoelectronic Technology, China Jiliang University, Hangzhou 310018, China*

We designed a broadband high-bit terahertz encoding metasurface structure. Through the principle of far-field scattering, we designed the corresponding matrix encoding to realize the control of terahertz waves, that is, extending the simple one-dimensional direction encoding to two-dimensional simultaneous encoding. Based on the matrix mode coding method, the coding metasurface can realize single-beam abnormal reflection, double-beam abnormal reflection and multi-beam abnormal reflection. At the same time, through the rotation arrangement pattern, we can obtain the reflected vortex beam. Our design provides a more flexible and high-degree-of-freedom manipulation method for terahertz wavefront regulation. At the same time, the design band can also be extended to microwave and visible light bands.

(Received July 1, 2022; accepted April 5, 2023)

Keywords: Metasurface, Reflection

1. Introduction

Metasurfaces are a branch of metamaterials [1-5]. It can be regarded as an ultra-thin two-dimensional plane, which is composed of a plurality of unit cells arranged at a microscopic level, that is, the sub-wavelength metamaterial unit structure is periodically or aperiodically extended on a certain plane, and then formed ultrathin metasurfaces [6-10]. The artificially fabricated metasurface has the advantages of electromagnetic 2π full-phase coverage regulation, and then completes functions such as abnormal deflection (or negative refraction), abnormal reflection and focusing [11-20].

The concept of a "metamaterial byte" was proposed by Giovampaola and Engheta [21], a metamaterial metasurface constructed using spatially mixed "digital metamaterial bits". This "digital metamaterial bit" is different from the information digital as we know it. It is composed of metamaterial unit structures (such as semiconductors with positive dielectric constant or metals with negative dielectric constant) according to different electric field characteristics. This "metamaterial byte" characterizes metamaterials with the parameters of the equivalent medium. Professor Cui proposed the concept of "encoded metamaterials"[22]. By designing metasurfaces based on this concept, devices with different functions can be obtained, such as propagating wave (PW) filters, absorbers, polarization converters, modulators, and holographic imaging devices [23-30]. The use of encoded metasurfaces also enables beam steering of free-space light. The 1-bit encoding metasurface is based on binary "0" and "1" digital states to replace two unit structures with "0" and "π" phase responses at specific frequencies, and simultaneously use these two unit structures for different arrange to control electromagnetic waves [31-34].

Currently, most designs of encoded metasurface devices focus on 1-bit encoded metasurfaces or 2-bit encoded metasurfaces. In order to achieve a higher degree of freedom in design, we use higher-bit coding units to construct coding metasurfaces to achieve different beam manipulation functions.

2. Far-field beam steering theory of encoded metasurface

In order to realize the beam regulation of electromagnetic waves, the traditional phased array antenna principle can realize the abnormal deflection of the beam in different interfaces, which is called the principle of far-field scattering. Coding metasurfaces refer to assigning binary numerical designations to the units that make up the coding metasurfaces. For the 1-bit encoding metasurface, it is composed of two units with a phase difference of exactly 180°, and the two units are assigned "0" and "1" respectively. In the same way, the 2-bit encoding metasurface is composed of 4 units, and the phase difference of the four units is 90° in turn, which are represented by "00", "01", "10", and "11" in sequence. For the 3-bit encoding metasurface, it is composed of 8 kinds of units, and the phase difference is 45° in turn. Eight 3-bit cells are represented by "000", "001", "010", "011", "100", "101", "110", "111".

Take the coding metasurface composed of m×n square grids of the same size and size P as an example, as shown in Fig.1. Each grid consists of sub-arrays that are crossed by "0" or "1" units, that is, the encoding period along the X and Y directions is 2P, and the transmitted phase φ(m,n). When the plane wave is perpendicularly incident along the -Z direction, the far-field scattering of the transmitted light of the metasurface can be expressed as [22]

$$F(\theta,\varphi)=f_e(\theta,\varphi)\sum_{m=1}^{M}\exp\{-i\varphi(m,n)-ik_0P\sin\theta[(m-1/2)\cos\varphi+(n-1/2)\sin\varphi]\} \quad (1)$$

Here, the wave vector is $k_0=\lambda/2\pi$. θ is the elevation angle, and ϕ is the azimuth angle. $f_e(\theta,\varphi)$ represents the radiation pattern of the unit structure. Assuming that the encoding period along the X direction is Γ_x and the encoding period along the Y direction is Γ_y, the above formula can be rewritten as

$$F(\theta,\varphi)=\sum_{m=1}^{M}\sum_{n=1}^{N}\exp\{-i\varphi(m,n)-i[k_0\frac{\Gamma_x}{2}\left(m-\frac{1}{2}\right)\sin\theta\cos\varphi+[k_0\frac{\Gamma_x}{2}\left(n-\frac{1}{2}\right)\sin\theta\cos\varphi]\} \quad (2)$$

Based on the transmission phase φ(m,n) of each cell being 0 or π, one can obtain

$$F(\theta,\varphi)=\sum_{m=1}^{M}\exp\left\{-i\left[k_0\frac{\Gamma_x}{2}\left(m-\frac{1}{2}\right)\sin\theta\cos\varphi+m\pi\right]\right\}\sum_{n=1}^{N}\exp\left\{-i\left[k_0\frac{\Gamma_y}{2}\left(n-\frac{1}{2}\right)\sin\theta\cos\varphi+n\pi\right]\right\} \quad (3)$$

It can be further obtained as

$$|F(\theta,\varphi)|=MN\cdot\sin c\left[m\pi\left(p+\frac{1}{2}\right)-\frac{m}{4}k_0\Gamma_x\sin\theta\cos\varphi\right]\cdot\sin c\left[n\pi\left(q+\frac{1}{2}\right)-\frac{n}{4}k_0\Gamma_y\sin\theta\cos\varphi\right] \quad (4)$$

where p， q=0,±1,±2.....The far-field intensity |F(θ,ϕ)| reaches the first extreme value and needs to meet the following conditions as

$$\phi=\pm tan^{-1}\frac{\Gamma_x}{\Gamma_y}and\phi=\pi\pm tan^{-1}\frac{\Gamma_x}{\Gamma_y} \quad (5)$$

$$\theta=sin^{-1}\left(\frac{2\pi}{k_0}\sqrt{\frac{1}{\Gamma_x^2}+\frac{1}{\Gamma_y^2}}\right) \quad (6)$$

The far-field scattering theory is derived from the 1-bit encoding metasurface, and also applies to 2-bit and 3-bit encodings. θ is the elevation angle of far field scattering , and ϕ is the azimuth angle of far field scattering for encoding metasurface.

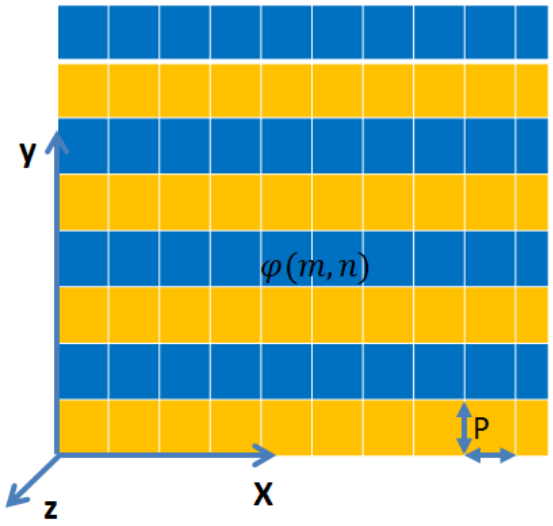

Fig. 1. Schematic diagram of encoding metasurface (color online)

3. Optimal design of multi-bit coding metasurface element structure

The level of 2π phase modulation is an important design condition that affects the efficiency of encoded metasurface. By using a higher level of phase modulation, the step-off of the phase profile is smoother. Therefore, based on the conventional 2-bit coding metasurface, we design a 3-bit coding metasurface working at 9.9-10.1THz. The metasurface is composed of a three-layer structure of metal-dielectric base layer and metal resonant layer. By changing the structural parameter r of the resonant unit, we optimized the unit structure that satisfies the phase condition of the high-bit encoding metasurface, and studied the electromagnetic regulation function of the response frequency band. Fig. 2 is a 3D schematic diagram of the metasurface unit structure proposed in this study. After careful design, the substrate and the resonant structure are both composed of gold. The thickness of the interlayer dielectric material is h1=1.6μm, and the dielectric constant is εr=2.65. In this design, other geometric parameters of the cell structure are shown in Fig. 3. The length and width of the cell are equal to the period p=10μm, and the thicknesses of the base metal layer and the resonant metal layer are both h=0.2μm. Due to the isotropic design of the resonant unit structure, the encoding metasurface can realize the regulation of anomalous refraction for both linearly polarized TE and TM waves. Taking the structural parameter r of the circular resonant unit as a variable, when the terahertz wave is vertically incident on the surface of the structure, by changing the radius r of the resonant unit, different unit structures that satisfy the phase condition can be obtained. Fig. 3 shows the reflection phase and reflection amplitude for different metal resonant disk diameters. According to the requirements of the phase gradient, 8 groups of cells "0", "1", "2", "3", "4", "5", "6" and "7" in this frequency band are designed. The coding unit with the adjacent reflection phase difference of 45° can be clearly seen from Figure 3(b). In the broadband range, the eight groups of

cells all have excellent reflection coefficients greater than 0.9 and a phase difference of approximately 45°. The dimensions of the radii r corresponding to cells "0", "1", "2", "3", "4", "5", "6" and "7" are r0=4.76μm, r1=4.45μm, r2=4.27μm, r3=4.12μm, r4=3.93μm, r5=3.61μm, r6=1.9μm, r7=5μm. We used the parameter scanning method to obtain the optimal geometric structure parameters.

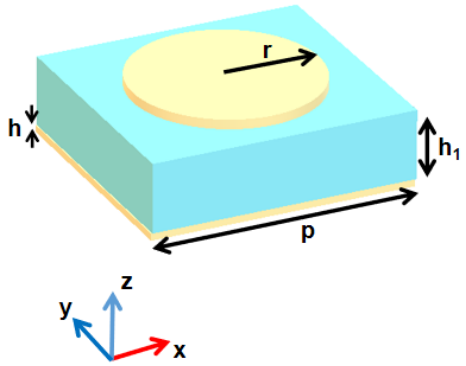

Fig. 2. 3D schematic diagram of the metasurface cell structure (color online)

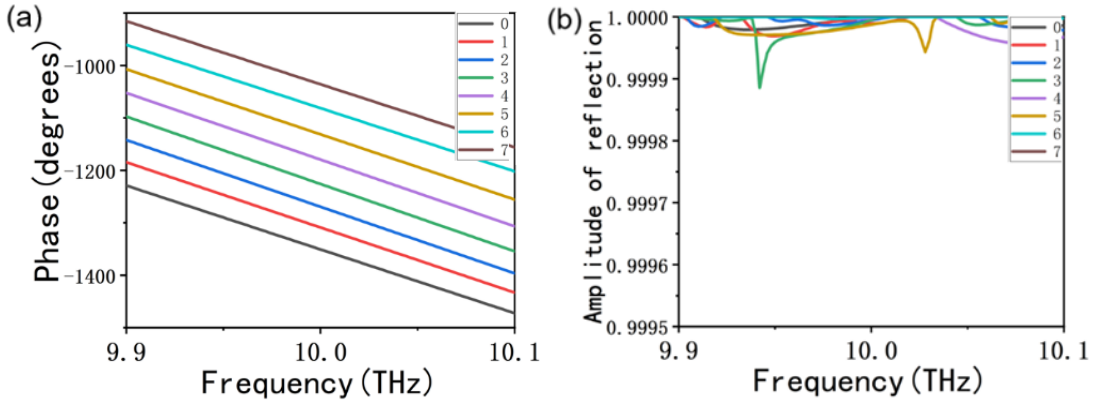

Fig. 3. Reflection phase shift and reflection amplitude of cell structure (a) co-polar reflection phase shifts and (b) co-polar reflection amplitudes of the eight elements (color online)

4. Abnormal beam reflection with encoding metasurface

We use 3-bit digital encoding to efficiently design the basic sequence of digital metasurfaces. We first designed the basic sequence consisting of 16×16 particles as S1=01234567..., and the sequence consisting of 16×16 particles as S2=0011223344556677.... Fig. 3(a) is the XY plane view (i) of the basic sequence supergrating S1 and the XY plane view (ii) of the basic sequence supergrating S2. As shown in Fig. 4(b), each color bar represents a group of corresponding coding cells. For metasurfaces with periodic arrangement of sequences S1 and S2, the far-field angle of electromagnetic waves is determined by the metasurface period of the gradient basic sequence of the arrangement. In this design, the unit structure length is p=10μm, then the period of the basic sequence S1 and the basic sequence S2 are Λ1=8p=80μm and Λ2=16p=160μm, respectively. According to Eq.(6) at 10THz, the theoretical anomalous scattering angles of the encoded metasurfaces of sequences S1 and S2 can be calculated to be 22.02° and 10.81°, respectively. As can be seen from Fig. 4(c)(i) and Fig. 4(c)(ii), the simulated scattering angles of the encoding metasurfaces S1 and S2 are 22.0° and 10.3°, respectively. The theoretical calculation results are basically consistent with the numerical simulation results. The designed encoded metasurface has precise angle control performance for a single beam of anomalous reflected waves, and our designed encoded metasurface grating can ideally manipulate electromagnetic waves. We used the finite integral method to calculate the near field distribution and far field scattering characteristics of the coded metasurface.

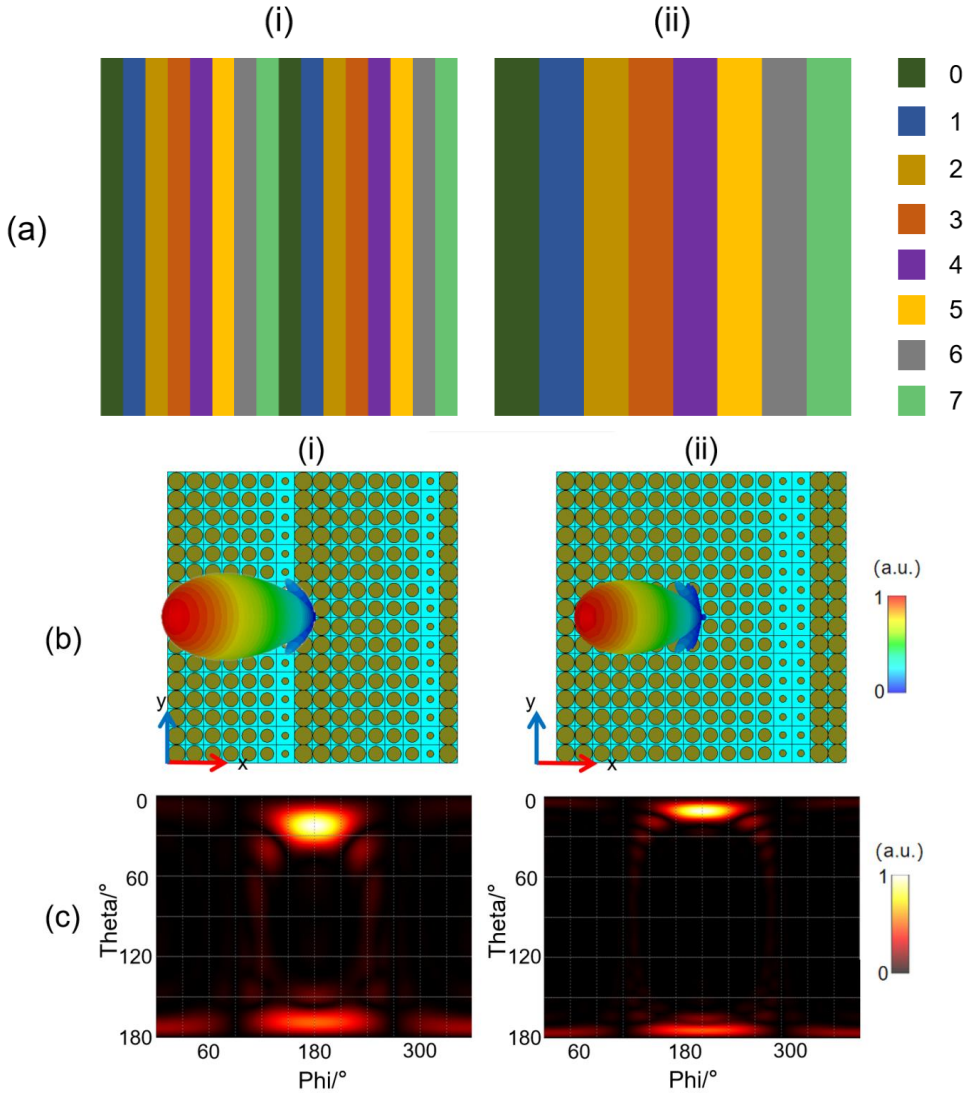

Fig. 4. (a)Coding sequences of encoding metasurfaces S1 and S2, (b)3D and (c)2D electric field maps (color online)

Based on the above eight groups of basic cells, we select the 0 and 4 groups of encoded particles to design a new sequence, which is the sequence S3=0044 composed of 16×16 particles. We further designed a sequence of 16×16 particles S4=00004444.... It can be seen that compared with the basic sequences S1 and S2, the codes of sequences S3 and S4 do not contain 6 groups of coded particles other than 0 and 4, and belong to 1-bit coding sequences. Fig. 5(a) is an XY plane view (i) of the basic sequence supergrating S3 and an XY plane view (ii) of the basic sequence supergrating S4. As shown in Fig. 5(b), each color bar represents a group of corresponding coding cells. For the metasurface whose sequence is S3 and S4 periodically arranged, the far-field angle of the electromagnetic wave is determined by the metasurface period of the gradient basic sequence of the arrangement. In this design, the length of the unit structure is p=10μm, then the periods of the basic sequence S3 and the basic sequence S4 are $\Lambda 3=4p=40\mu m$ and $\Lambda 4=8p=800\mu m$, respectively. The theoretical anomalous scattering angles of the encoded metasurfaces of sequences S3 and S4 can be calculated to be 48.59° and 22.02°, respectively. From the scattering in Fig. 5(b), it can be found that both sequences S3 and S4 can obtain two main lobes that are symmetrical about the Z axis. The scattering angles of the light scattered by the encoded metasurface S3 are 47.9° and 47.8° with respect to the z-axis, respectively. The scattering angles of the light scattered by the encoded metasurface S4 are 21.0° and 22.0° with respect to the z-axis, respectively.

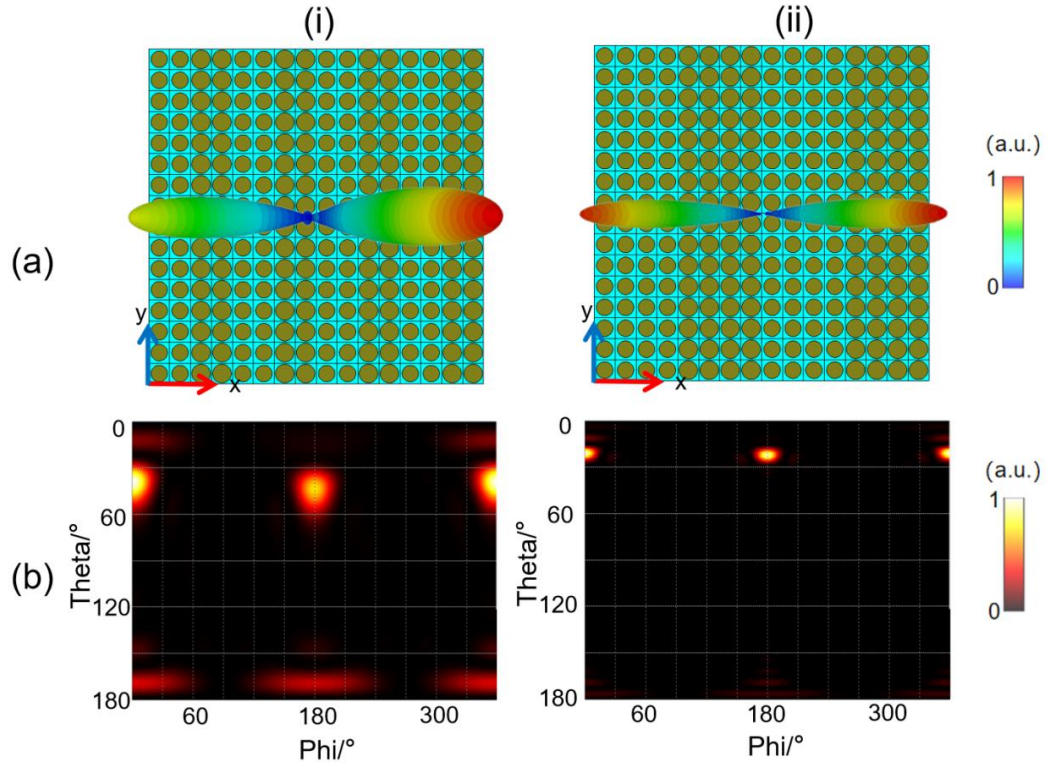

Fig. 5. (a)3D scattering and (b)2D electric field maps of encoded metasurfaces S3 and S4 (color online)

Next, we propose the cross-encoding patterns, and a matrix-like M sequence of checkerboard encoding patterns is demonstrated. The matrix mode M can be expressed as

$$M = \begin{bmatrix} A & B \\ B & A \end{bmatrix} \tag{7}$$

where A and B are "m×n" submatrices, and the encoded particles in A or B are the same unit particle. A and B can be expressed as

$$A_{m\times n}=\begin{bmatrix} 0 & \cdots & 0 \\ \vdots & \ddots & \vdots \\ 0 & \cdots & 0 \end{bmatrix}; B_{m\times n}=\begin{bmatrix} 4 & \cdots & 4 \\ \vdots & \ddots & \vdots \\ 4 & \cdots & 4 \end{bmatrix} \tag{8}$$

A number in the sub-matrix corresponds to a unit particle of the code, and this matrix encoding method is denoted as S_nXS_mY, where n and m also represent unit particles the number in the X and Y directions. For example, the matrix encoding S_3XS_3Y has the same encoding period in the X and Y axis directions. Next, we specifically study the 4×4 A and B matrix form as

$$A_{4\times 4}=\begin{bmatrix} A_1 & A_2 \\ A_3 & A_4 \end{bmatrix}; B_{4\times 4}=\begin{bmatrix} B_1 & B_2 \\ B_3 & B_4 \end{bmatrix} \tag{9}$$

The sub-matrix in the matrix A and B is a 2×2 square matrix, and the elements of the coding unit are the same.

The new sequence can be defined as S_XmS_Yn, where m and n refer to the number of coding unit elements in one cycle along the X and Y axes, respectively. For example, the sub-arrays in matrix A and B are

$$A_1=A_2=\begin{bmatrix} 0 & 0 \\ 0 & 0 \end{bmatrix} \tag{10}$$

$$A_3=A_4=\begin{bmatrix} 2 & 2 \\ 2 & 2 \end{bmatrix} \tag{11}$$

$$B_1=B_2=\begin{bmatrix} 4 & 4 \\ 4 & 4 \end{bmatrix} \tag{12}$$

$$B_3=B_4=\begin{bmatrix} 6 & 6 \\ 6 & 6 \end{bmatrix} \tag{13}$$

When the matrix pattern sequence is S_X2S_Y4, the coding unit elements along the X axis are "0" and "4" or "2" and " 6", and the coding unit elements in the Y-axis direction are four elements "0", "2", "4", and "6". When the terahertz plane wave is perpendicular to the encoding metasurface, it is divided into four beams, two beams and one beam, respectively, as shown in Fig. 6.

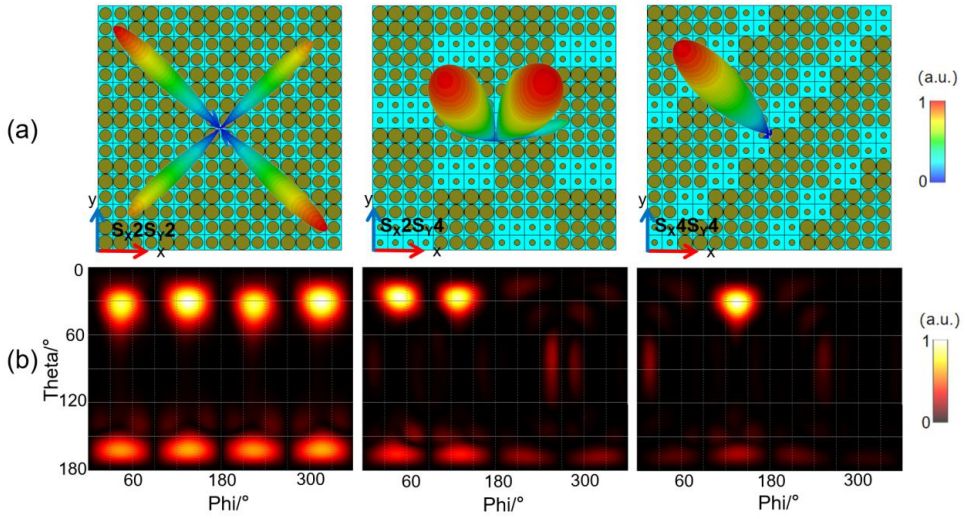

Fig. 6. (a)3D and (b)2D electric field distribution maps of matrix checkerboard-encoded metasurfaces (color online)

5. Coded metasurface vortex beam

In order to demonstrate the multi-functional effect of this design with highly flexible regulation of electromagnetic waves, we continue to perform rotational encoding based on the unit structure to generate vortex beams with topological charges of 1 and 2, respectively. When an electromagnetic wave with an incident frequency of 10 THz is incident vertically along the -Z direction, the far-field distribution of scattered light is shown in Fig.7. From the scattered light intensity distribution, it can be seen that the light intensity at the center of the encoded metasurface is close to 0, and the light intensity distribution is in the form of a doughnut, and the corresponding phase is in a spiral shape, which is in line with the characteristics of a vortex beam, as shown in Fig. 6(b). Fig. 6(ii) shows the scattered light intensity distribution and phase distribution with a topological charge of 2. It can be seen that the encoding metasurface in this design can generate terahertz wave vortex beams, and realize the multi-functional free manipulation of terahertz waves.

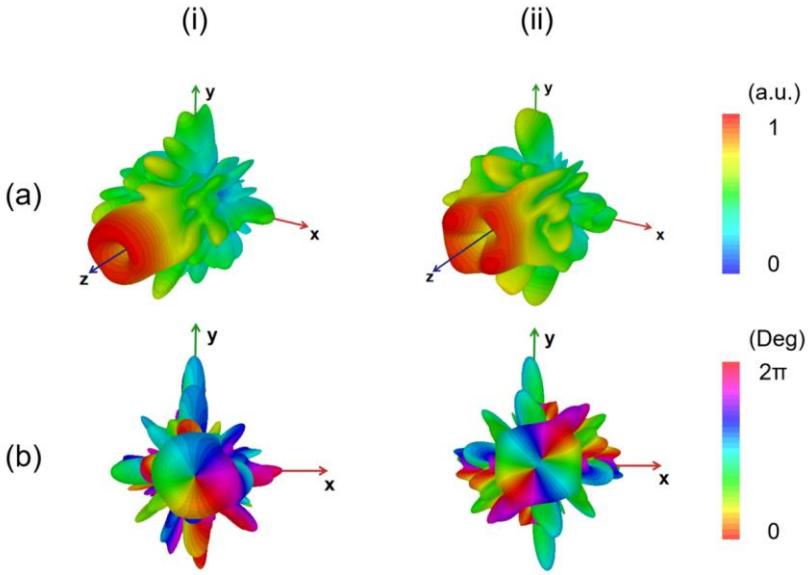

Fig. 7. Far-field scattering images (a) and phase images (b) of the encoded metasurface with topological charges l=1(i) and l=2(ii), respectively (color online)

Although our work is based on the numerical simulation, it is feasible to fabricate such encoding metasurface. Compared with previous metasurface devices in the visible and infrared spectrum, the size of the metasurface unit in the terahertz band is larger and therefore simpler to manufacture. The metal structure can be processed using conventional standard electron beam lithography (EBL) and lift-off techniques. The complete processing flow can be divided into the following steps, including coating spin glue, electron beam lithography, dry etching, debonding, and preparation process.

6. Conclusions

The control of terahertz waves is realized by designing the corresponding matrix encoding based on the principle of far-field scattering, that is, extending the simple one-dimensional (only along the X or Y direction) encoding to two-dimensional simultaneous encoding. To achieve multi-beam scattering regulation, we propose a matrix pattern encoding method. The coding metasurface designed by us can not only realize the regulation of single-beam anomalous reflection beams, but also realize multi-beam anomalous reflection phenomena. This matrix-encoded pattern approach may hold promise for engineering applications in information communication, imaging, and smart surfaces, and so on.

References

[1] X. He, Carbon **82**, 229 (2015).
[2] X. He, X. Zhong, F. Lin, W. Shi, Opt. Mater. Express **6**, 331 (2016).
[3] Xiaoyong He, Feng Liu, Fangting Lin, Wangzhou Shi, Opt. Lett. **46**, 472 (2021).
[4] Xiaoyong He, Feng Liu, Fangting Lin, Wangzhou Shi, J. Phys. D: Appl. Phys. **54**, 235103 (2021).
[5] Jun Peng, Xiaoyong He, Chenyuyi Shi, Jin Leng, Fangting Lin, Feng Liu, Hao Zhang, Wangzhou Shi, Physica E **124**, 114309 (2020).
[6] X. Jing, S. Jin, Y. Tian, P. Liang, Q. Dong, L. Wang, Optics & Laser Technology **48**, 160 (2013).
[7] X. Jing, Y. Xu, H. Gan, Y. He, Z. Hong, IEEE Access **7**, 144945 (2019).
[8] L. Jiang, B. Fang, Z. Yan, J. Fan, C. Qi, J. Liu, Y. He, C. Li, X. Jing, H. Gan, Z. Hong, Optics & Laser Technology **123**, 105949 (2020).
[9] H. Lv, X. Lu, Y. Han, Z. Mou, S. Teng, Optics Letters **44**(10), 2518 (2019).
[10] H. Wang, L. Liu, C. Zhou, J. Xu, M. Zhang, S. Teng, Y. Cai, Nanophotonics **8**(2), 317 (2019).
[11] Jinxing Li, Yueyi Yuan, Qun Wu, Shah Nawaz Burokur, Kuang Zhang, Chin. Opt. Lett. **19**, 100501 (2021).
[12] S. Teng, Q. Zhang, H. Wang, L. Liu, H. Lv, Photonics Research **7**(3), 246 (2019).
[13] M. R. Akram, G. Ding, K. Chen, Y. Feng, W. Zhu, Advanced Materials **32**, 1907308 (2020).
[14] J. Zhang, X. Wei, I. D. Rukhlenko, H.-T. Chen, W. Zhu, ACS Photonics **7**(1), 265 (2020).
[15] Haoyu Wang, Zhiyu Zhang, Kun Zhao, Wen Liu, Pei Wang, Yonghua Lu, Chin. Opt. Lett. **19**, 053601 (2021).
[16] Bo Fang, Zhiyu Cai, Yandong Peng, Chenxia Li, Zhi Hong, Xufeng Jing, Journal of Electromagnetic Waves and Applications **33**(11), 1375 (2019).
[17] Fang, B, Li, B, Peng, Y, Li, C, Hong, Z, Jing, Microw. Opt. Technol. Lett. **61**, 2385 (2019).
[18] Weimin Wang, Xufeng Jing, Jingyin Zhao, Yinyan Li, Ying Tian, Optica Applicata **47**(2), 183 (2017).
[19] L. Jiang, B. Fang, Z. Yan, Microwave and Optical Technology Letters **62**(6), 2405 (2020).
[20] Yi Zhao, Qiuping Huang, Honglei Cai, Xiaoxia Lin, Hongchuan He, Hao Cheng, Tian Ma, Yalin Lu, Chin. Opt. Lett. **19**, 073602 (2021).
[21] Della Giovampaola C, Engheta, Nature Materials **13**(12), 1115 (2014).
[22] T. J. Cui, M. Q. Qi, X. Wan, Light: Science & Applications **3**(10), e218 (2014).
[23] Hafiz Saad Khaliq, Inki Kim, Aima Zahid, Joohoon Kim, Taejun Lee, Trevon Badloe, Yeseul Kim, Muhammad Zubair, Kashif Riaz, Muhammad Qasim Mehmood, Junsuk Rho, Photonics Research **9**(9), 09001667 (2021).
[24] Matthew Parry, Andrea Mazzanti, Alexander Poddubny, Giuseppe Della Valle, Dragomir N. Neshev, Andrey A. Sukhorukov, Advanced Photonics **3**(5), 055001 (2021).
[25] Ai Du, Yi Ma, Mingfang Liu, Zhihua Zhang, Guangwei Cao, Hongwei Li, Ling Wang, Peijian Si, Jun Shen, Bin Zhou, High Power Laser Science and Engineering **9**(2), 02000e14 (2021).
[26] Tina Ebert, René Heber, Torsten Abel, Johannes Bieker, Gabriel Schaumann, Markus Roth, High Power Laser Science and Engineering **9**(2), 02000e24 (2021).
[27] Xinhua Xie, Yunpei Deng, Steven L. Johnson, High Power Laser Science and Engineering **9**(4), 04000e66 (2021).
[28] X. Jing,X. Gui, P. Zhou, Z. Hong, Journal of Lightwave Technology **36**(12), 2322 (2018).
[29] R. Xia, X. Jing, X. Gui, Y. Tian, Optical Materials Express **7**(3), 977 (2017).
[30] M. R. Akram, M. Q. Mehmood, X. Bai, R. Jin, M. Premaratne, W. Zhu, Advanced Optical Materials **7**, 1801628 (2019).
[31] J. Zhao, X. Jing, W. Wang, Y. Tian, D. Zhu, G. Shi, Optics and Laser Technology **95**, 56 (2017).
[32] J. Li, R. Jin, J. Geng, X. Liang, K. Wang, M. Premaratne, W. Zhu, IEEE Transactions on Antennas and Propagation, **67**(4), 2442 (2019).
[33] Xiaoyong He, Wenhan Cao, Opt. Mater. Express **13**, 413 (2023).
[34] Xiaoyong He, Fangting Lin, Feng Liu, Wangzhou Shi, Nanophotonics **11**(21), 4705 (2022).

*Corresponding author: lichenxiacjlu@163.com